Egyptian Journal of Chemistry
http://ejchem.journals.ekb.eg/

Tellurium/Vanadate Doped Hydroxyapatite Nano-Scaffold Carrier for Doxorubicin Colon Cancer Targeting

Mayssa Abdel Hady[1*], M.K. Ahmed[2,3]

[1]*Department of Pharmaceutical Technology, National Research Center, Dokki, Giza, Egypt*
[2]*Department of Physics, Faculty of Science, Suez University, Suez 43518, Egypt*

Abstract

Designing specific chemotherapy delivery systems that target cancer cells is widely studied nowadays. Different substitutions of tellurium (Te)/vanadate (V) doped hydroxyapatite (HAP) have been suggested to be used as a carrier scaffold for doxorubicin (DOX). In contrast, the ultimated scaffold is coated with chitosan (CS) to be utilized and studied as a colon cancer therapy. Evaluation of DOX release explains the specific cleavage of DOX from CS-coated HAP at enteric pH in a controlled-release state. This formulation was studied with XRD and XPS to confirm composition elements and purity. As displayed from SEM micrographs, it can be illustrated that the morphological alterations and grain size of an average diameter of 0.5-2 µm for 1Te/V-HAP/DOX-CS. Further, it was observed that DOX shows a loading capacity of 99% for all the compositions. The cytotoxicity assay was assessed against HT-29 colorectal cell lines, implying that the activity of DOX loaded nanocomposite was maintained. Therefore, the present investigation recommended that the CS-coated Te/V-HAP/DOX is an excellent nominee for colon cancer treatment.

Keywords: Hydroxyapatite; Doxorubicin; Colon cancer; Drug delivery system

1. Introduction

Drug delivery systems have been widely studied recently due to their potent and safe properties and better bioactivity [1]. The therapy of choice nowadays is to prepare novel systems to treat different types of cancer owing to their managed and targeted drug release and their nontoxic, biodegradable, and biocompatible characterizations [2]. These carriers containing chemotherapy are developed to target tumor cells and minimize harm to normal cells [3]. Colon (the large intestine) cancer is recognized to be one of the most common neoplastic diseases with a high mortality rate. [4]. Lately, applying nanotechnology in performing drug delivery systems to treat colon cancer lead to an improvement in the penetration and accumulation of chemotherapeutic drugs into tumor cells; besides, it controlled the rate of drug release [5]. Hydroxyapatite is one of the most privileged drug carriers in delivery systems in colon cancer therapy [6]. Hydroxyapatite (HAP) is an inexpensive, safe, biodegradable, and bioactive inorganic material utilized widely in biomedical, particularly drug delivery [7]. However, the rate of pure HAP degradation limits its use solely [8]. Interestingly, the flexible structure of HAP to metal doping can control its biodegradable and bioactive properties [8, 9]. Besides, HAP was characterized by its excellent drug loading and release rate [10]. S. Dey et al. explained the role of nano-sized HAP of diameter range 10-100 nm in inhibiting colon cancer cells [11]. They demonstrated that the nanoparticles could penetrate cell membranes easily via endocytosis. Further, Y. Zhang et al. studied HAP and chitosan as an oral delivery system [12]. They showed that this combination improved the bioavailability and solubility of the carried drug. Chitosan (CS) is a biocompatible, biodegradable, and nontoxic cationic biopolymer [13]. Interestingly, It can be utilized as a coating compound in pharmaceutical delivery systems due to its corrosion stability and the easy formation of a uniform coat [14]. CS coat enhances the carrier material's cell attachment and biocompatibility [15].

*Corresponding author e-mail: ma.abdel-hady@nrc.sci.eg.;(Mayssa Abdel Hady).
EJCHEM use only: Received date 26 January 2023; revised date 07 February 2023; accepted date 07 February 2023
DOI:10.21608/EJCHEM.2023.189848.7518

Besides, CS could attach to the mucous membranes [12]. In addition, S. Wahba et al. [17], demonstrated the enhancement in bioavailability and biodegradability of the delivery system upon coating HAP with chitosan [16]. Moreover, J. Prakash et al. showed the enhancement of HAP porosity and bioactivity upon coating with CS.

Doxorubicin (DOX) is one of the anthracycline family that treats different types of tumors involving colon cancer; the main drawback of doxorubicin is its cardiotoxicity [18]. Hence, loading DOX on nanocarriers has been studied recently due to the advantage of targeting tumor cells and minimizing side effects [19]. S. Shang et al. showed the high loading capacity of DOX on the metal-doped HAP [20]. They explained that HAP has a high adsorption ability for drugs containing numerous functional groups. The dopant ion changed the spaces of the HAP crystalline structure leading to more loading capacity.

Tellurium is a trace and nonessential element [21]; it is an element of interest newly in biomedical purposes because of its antimicrobial potential and the ability to hinder cancer growth through the ROS mechanism [22]. M. Doering et al. [23] confirmed that Te-containing compounds are highly active in biological matrices and have remarkable activity against tumor cells. Moreover, Peng Du et al. [24]proved the ability of Te against colon cancer cells without harming normal cells. They explained that Te induced high levels of free radicals in cancer cells, which lead to cancer cell death; otherwise, normal cells that cannot influence this high level of free radicals. Vanadium (V) is a promising dopant metal ion widely studied in various biomedical applications [25]. Vanadium is proven to exert anticancer activity against human tumors, and it was explained that V affects the cell cycle and leads to cell arrest [26].

The main objective of the present study is the production of Te/V-HAP/DOX-CS and the evaluation of its cytotoxic activity against colorectal cell lines for the therapeutic application of doxorubicin through a targeted colon delivery.

2.1. Materials

Hydroxyapatite (HAP), Calcium chloride, ammonium phosphate, chitosan, vanadium oxide, and tellurium chloride were obtained from Loba, India.

2.2. Synthesis CS-HAP nanoparticle

A mixture of Chitosan, acetic acid, as well as deionized water in which the strength of chitosan was kept at 1 wt%, was prepared. The mixture was left for four hours to ensure the complete dissolving of chitosan. HAP suspension (1 wt%) was added dropwise, at a dropping rate of 1drop/sec^{-1} using a syringe controlled by a peristaltic pump, to the prepared chitosan solution to reach a 1:1 final volume ratio. pH of the final suspension was fined to pH 6.5 using 10 wt % NaOH. The samples were then washed with deionized water at least three times, followed by drying freely at room temperature for further assessments.

2. Characterization of prepared compounds

2.3. Characterization

X-ray diffraction analysis (XRD) was performed to distinguish compositional variation using a diffractometer (Pertpro, CuK1 radiation, l=1.5404, 45 kV, 40 mA, USA. The obtained compositions were analyzed using an X-ray photoelectron spectroscopy (XPS) instrument (Perkin-Elmer PHI 5600). The samples' morphology and roughness were assessed using a (FESEM) (QUANTA-FEG250, Netherlands).

The loading capacity of the formulated HAP was assessed using a range of doxorubicin concentrations from 5 mg/L up to 45 mg/L. Fixed amount of HAP (50 mg) was immersed in 50 mL doxorubicin solution for 48 hours at 25 oC and continuously shaken using a benchtop shaker. The filtrate solutions were collected through centrifugation. The residual concentrations were determined using UV-spectrophotometer (Shimadzu, Japan) at λmax 498 nm. Each test was performed in triplicate, then the average values with a standard deviation of less than 3.5 % was then evaluated. The amount of the loaded drug was calculated according to Eq.1.[27]

$$\text{Amount of loaded drug} = (A - B) / A \times 100 \quad \text{Eq. 1}$$

Where A and B represented the initial and final drug concentrations, respectively.

Using a USP Dissolution Apparatus II, the release behavior of doxorubicin was evaluated in vitro using 500 mL of dissolution medium with pH 2.1 PBS solution (made by dissolving 6.80 g of KH2PO4 and 2M HCl in 1000 mL of distilled water) for 2 h defined and then assayed in pH 7.4 PBS) maintained at 37±0.5°C and stirred at 50 rpm. One gram of the chitosan-coated and uncoated HAP suspension was added to the dissolving medium and put into a dialysis bag that was clamped shut at both ends. After 2 h, the pH of the PBS solution was filtered using a 100 mesh sieve and then changed to pH 7.4 for further testing. At regular intervals, 5 ml aliquots of the release medium were taken out and their drug concentration was then spectrophotometrically measured at 498 nm. Fresh media volumes in equal amounts replaced the deleted samples. Doxorubicin release cumulative percentages were plotted as a function of time. The studies were carried out three more times, and the

mean, and standard deviation was being used to represent the findings.

Relative release of doxorubicin was determined using Eq. (2):

Cumulative doxorubicin release (%) = Rt/L X 100 Eq. 2

Where, L and Rt represent the initial amount of doxorubicin-loaded and the cumulative amount of doxorubicin released at time t, respectively.

Colorectal Cancer cell line (HT-29) was purchased from Nawah Scientific Inc., (Mokatam, Cairo, Egypt). The obtained cells were well-maintained in DMEM solution having 100 mg/mL of streptomycin, 100 units/mL of penicillin, and 10% of heat-Inactivated fetal bovine serum in humidified, 5% (v/v) CO2 atmosphere at 37 °C.

Cell viability experiments were taken into consideration using the SRB assay. A suitable medium was used to incubate aliquots of 100 µL cell suspensions (5 x 103 cells) in 96-well microplates for 24 hours. The cells were then exposed to 100 µl of medium containing doxorubicin at various concentrations (0.01, 0.1, 1, 10, and 100 µg/ml) that was loaded with HAP. 150 µL of TCA (10%) was added to the cells at 4°C after 72 h to facilitate fixation. The TCA solution was discarded after the fixation procedure had taken one hour, and distilled water was used to wash the cells five times. Aliquots of a 70% LSRB solution were inserted and kept at 25°C in complete darkness for 10 min (0.4% w/v). The plates were given another wash with acetic acid (1%) and enough time to dry overnight. TRIS (10 mM) was added to 150 µL of the sample to remove protein-bound SRB staining. A microplate reader equipped with the BMG LABTECH-FLUOstar Omega was used to quantify absorbance at 540 nm.

3. Results and discussion

3.1. XRD analysis

Fig. 1 shows the X-ray diffraction of different contributions of Te/V-HAP composition. The spectra of all substitutions show intense peaks at the same angles at 2Θ= 26˚, 31.8˚, 33.6˚, 46.4˚, 49.7˚ that are assigned for the specific HAP crystal planes (002), (211), (300), (222), and (213) respectively [28]. The same XRD patterns represent the purity of HAP; however, the successful substitution is characterized by decreasing peak intensities with increasing Te substitution due to the alteration in HAP crystal lattice structure [29].

XPS spectra of Te/V-HAP@CS-DOX are demonstrated in Fig. 2, while the binding energy values of the peaks and the atomic percentage are reported in Table 1. XPS is used to determine the elements of the composition and ensure the bonding within the composition [30]. Fig 2a shows the composition's survey scan, which shows the significant bands attributed to the elements O, P, V, Te, Ca, and N. The N 1s peak in the survey scan confirms the presence of the nitrogen-containing compounds DOX and CS [31, 32]. This survey proves the uniform loading of DOX within HAP as well as the even substitution of Te and V ions within HAP and the uniform coating with chitosan. Fig 2b shows the O 1s scan deconvoluted to three bands assigned to Te-O, P-O, and N-O at binding energy 531.3 eV, 531.9 eV, and 532.7 eV, respectively [33-36].

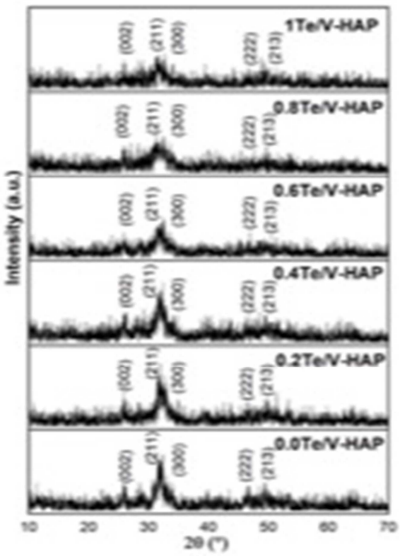

Fig. 1: XRD patterns of different contributions of Te/V-HAP

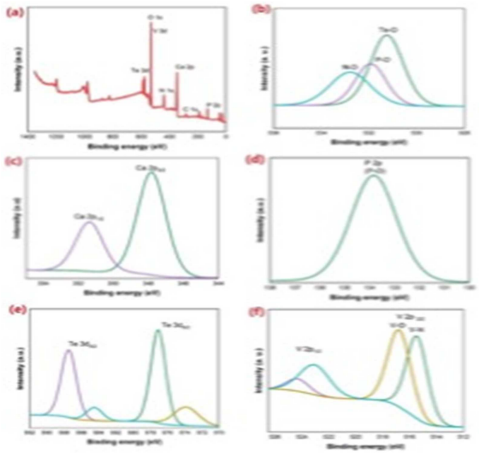

Fig. 2: XPS patterns of Te/V-HAP@CS-DOX: (a) survey scan, (b) O 1s scan, (c) Ca 2p, (d) P 2p, (e) Te 3d, (f) V 2p

Further, Fig 2c shows the Ca 2p scan presenting two significant peaks for Ca $2p_{3/2}$ and Ca $2p_{1/2}$ at

347.7 eV and 351.3 eV [37, 38]. Moreover, Fig 2d represents the single peak of the P 2p scan at binding energy 133.8 eV [30, 39]. Fig. 2e demonstrates the two significant peaks of the Te 3d scan, which separated with 10 eV values appearing at 577.2 eV and 587.4 eV that ascribed for Te $3d_{5/2}$ and Te $3d_{3/2}$ [40].

The V 2p scan is shown in Fig. 3f, presenting the specific peaks of V $2p_{3/2}$ and V $2p_{1/2}$ at a binding energy of 515.8 eV and 523.1 eV for V-N (V^{4+}) and 516.9 eV and 524.4 eV for V-O (V^{5+}) [41-43].

Table 1: XPS influential bands for Te/V-HAP/CS-DOX

Bond	Binding energy (eV)	Atomic (%)	Assignment	Ref.
P 2p	133.8	100	P 2p1/2	[30, 39]
V 2p	515.8	36.91	V-N 2p3/2	[41, 42]
	516.9	37.91	V-O 2p3/2	[41, 43]
	523.1	19.19	V-N 2p1/2	[41, 42]
	524.4	5.99	V-O 2p1/2	[41, 43]
Ca 2p	347.7	68.19	Ca 2p3/2	[37, 38]
	351.3	31.81	Ca 2p1/2	[37, 38]
O 1s	531.3	35.72	Te-O	[36]
	531.9	21.08	P-O	[33, 34]
	532.7	43.12	N-O	[35]
Te 3d	577.2	45.13	Te 3d5/2	[40]
	587.4	33.31	Te 3d3/2	[40]

3.3. Morphological features

Fig. 3 shows the SEM micrographs of different contributions of Te/V-HAP before loading DOX. Fig. 3a shows the aggregated pattern of HAP with an average diameter of 0.3-0.5µm. Further, 0.4Te/V-HAP is presented in Fig. 3b, in which the clustered particles of HAP are somehow detangled with a grain size of 0.1-0.3 µm. Moreover, Fig. 3c shows 0.6Te/V-HAP demonstrating an enhanced porous structure of HAP with a diameter of 0.3 µm. Furthermore, the 1Te contribution remarkably improves HAP porosity, explained in Fig. 3d showing a particle size of 0.2 µm. The highest Te substitution is 1.2Te/V-HAP, shown in Fig. 3e, showing a fluffy and highly porous structure with the lowest average grain diameter of 0.1 µm. This structure alteration and grain size reduction due to ion substitution helps in the better loading and release manner of DOX from HAP [11, 20].

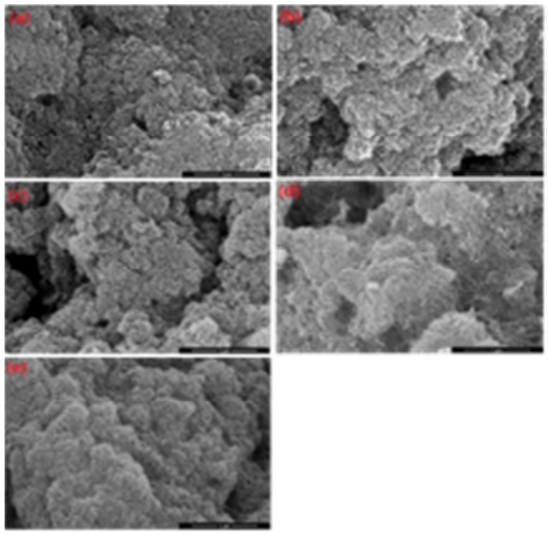

Fig. 3: FESEM patterns of Te/V-HAP: (a) 0.0Te/V-HAP, (b) 0.4Te/V-HAP, (c) 0.6Te/V-HAP, (d) 1Te/V-HAP, (e) 1.2Te/V-HAP.

3.4. Loading capacity of doxorubicin as drug

The loading capacity of doxorubicin on different HAP composites is shown in Table 2. Whereas loading behaviour of doxorubicin on the HAP composite is illustrated in Fig. 4. It was apparent from the results that doxorubicin has a high loading capacity on the HAP, showing a high loading level of around 99% regardless of the composition of Te doped HAP. All loadings showed a linear relationship with increasing initial concentration. The high loading capacity of doxorubicin is attributed to either the covalent bonding between the drug and the surface of the composite; or to the hydroxyl group of HAP, which interacts with the drug molecules via hydrogen bonds, or simply by adsorption via electrostatic bonding [6, 44]. This bonding enhances the drug's loading and releasing behavior [6].

Table 2: Doxorubicin loading capacity on Te/V-HAP

Te Ratio	% loading
0	99.35583
0.2	99.26375
0.4	99.445
0.6	99.44458
0.8	99.13292
1	99.18958
1.2	99.21375

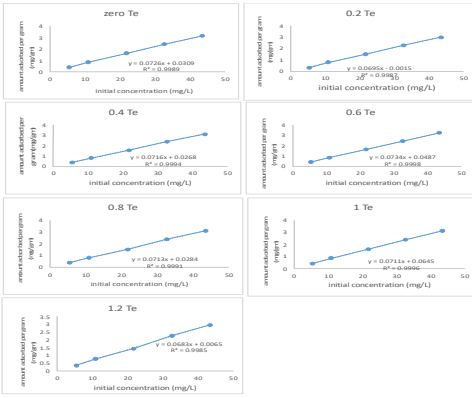

Fig. 4 Relationship between initial doxorubicin concentration and the amount adsorbed per gram HA

3.5. In vitro Drug cumulative release

The release profiles for doxorubicin from chitosan-coated and non-coated HAP composites are shown in Fig. 5 and 6, respectively. It was shown from the profiles that both coated, and non-coated composites are shown almost no release in the acidic pH period of the two hours except for formula 0Te, 0.4Te, 0.6Te, and 1.2Te in the case of coated composites and formula 0Te, 0.4Te and 1.2Te in case of non-coated composites. After 2 hours, we found a slow release pattern for all formulations except for formula 0Te, which achieved almost complete release at 72 hours. These findings came contrary to previous results by Kundu et al., who stated that the release of doxorubicin is not dependent on pH [44]. The slow release of doxorubicin in acidic conditions was also contrary to work done by Kim et al., who concluded that acidic conditions are more favorable for the release of the drug [27]. The slow release of doxorubicin from HAP composites with Te could be attributed to the possible interaction between the drug and the high loading of the drug on the composites. This could be beneficial in the case of targeting colon cancer.

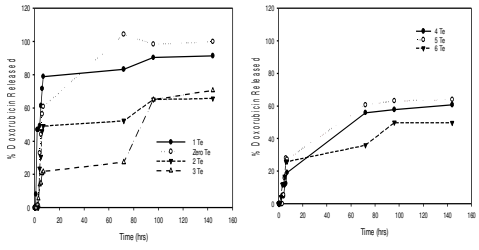

Fig. 5 Release profiles of doxorubicin from non-coated HAP composites

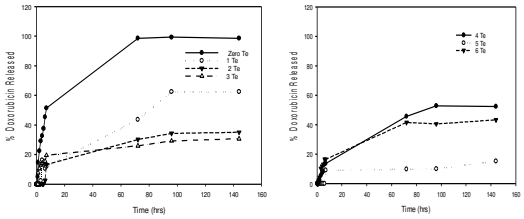

Fig. 6 Release profiles of doxorubicin from chitosan coated HAP composites

3.6. In vitro cytotoxicity studies

Fig. 7 and Fig. 8 show the cytotoxicity assay of Te/V-HAP@DOX-CS composition towards the HT-29 colorectal cell line. The toxicity of the least released DOX concentration against the HT-29 cell line is high, with an average toxicity of 95%. Besides, the low 50% inhibitory concentration (IC50) value of DOX of 0.26 µg/ml explains the high toxic effect of DOX against the HT-29 cell line. These cytotoxicity results confirm the potency of DOX regardless of the loading process on metal-doped HAP and the coating process with CS.

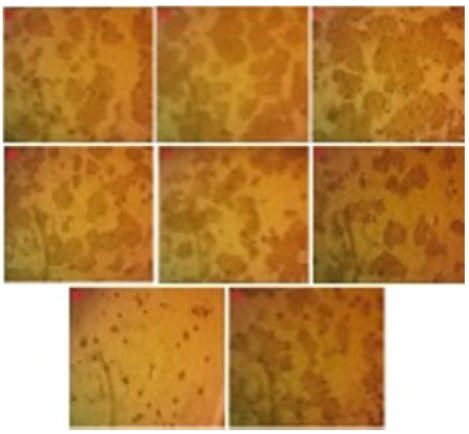

Fig. 7: HT-29 colorectal cell lines cytotoxicity assay

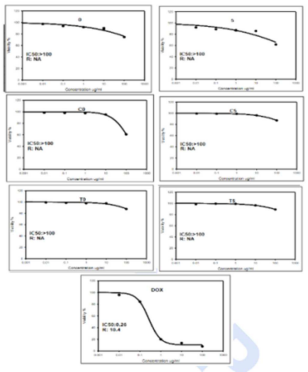

Fig. 8: bahavior of HT-29 colorectal cell lines cytotoxicity assay

4. Conclusion

Te/V HAP composition with different contributions of Te ions, then load DOX onto these different compositions was prepared. Each composition was divided into two parts: one was coated with chitosan (CS), and the other was not covered. DOX has a high resilience of 99% for all compositions. All coated and uncoated formulations were being studied and analyzed for serving as a drug delivery system for the anticancer drug doxorubicin for the treatment of colon cancer. The biological assay is performed against HT-29 colorectal cell lines, and the viability of doxorubicin showed high potency against the cell line. However, it undergoes loading and coating procedures with an average viability value of about 95%. XRD confirms pure HAP crystal structure and successful Te substitution. The elemental composition was analyzed with XPS, which showed the even distribution within the composition. SEM images showed the change in morphological structure and particle size with an average diameter of 0.5–2 m that occurred upon HAP-1Te ion substitution, thereby improving the loading and release behavior of DOX. After 2 hours, a slow release of DOX was observed. This can be considered to be a significant step forward in therapeutic application of the CS-coated Te/V-HAP/DOX for the treatment of colon cancer.

References

1. Ali W. Al-Ani et al., *Development of a nanostructured double-layer coated tablet based on polyethylene glycol/gelatin as a platform for hydrophobic molecules delivery*. Egyptian Journal of Chemistry, 2021, 64, p. 1759 - 1767.
2. Khaled R. Mohame et al., *Fabrication of hydroxyapatite–aluminum silicate/chitosan-elatin biocomposites with In-Vitro application by preosteoblast cells (MC3T3-E1).* Egyptian Journal of Chemistry, 2022, 65, p. 79 - 95.
3. Li, H., et al., *Preparation and properties of carbon nanotube (Fe)/hydroxyapatite composite as magnetic targeted drug delivery carrier.* Materials Science and Engineering: C, 2019. **97**: p. 222-229.
4. Khoshtabiat, L., A. Meshkini, and M.M. Matin, *Fenton-magnetic based therapy by dual-chemodrug-loaded magnetic hydroxyapatite against colon cancer.* Mater Sci Eng C Mater Biol Appl, 2021. **127**: p. 112238.
5. Taşdelen, B., S. Erdoğan, and B. Bekar, *Radiation synthesis and characterization of chitosan/hyraluronic acid/hydroxyapatite hydrogels: Drug uptake and drug delivery systems.* Materials Today: Proceedings, 2018. **5**(8): p. 15990-15997.
6. Guo, Y.-P., et al., *Hydrothermal fabrication of mesoporous carbonated hydroxyapatite microspheres for a drug delivery system.* Microporous and Mesoporous Materials, 2012. **155**: p. 245-251.
7. Heng, C., et al., *Fabrication of luminescent hydroxyapatite nanorods through surface-initiated RAFT polymerization: Characterization, biological imaging and drug delivery applications.* Applied Surface Science, 2016. **386**: p. 269-275.
8. Singh, G., S.S. Jolly, and R.P. Singh, *Cerium substituted hydroxyapatite mesoporous nanorods: Synthesis and characterization for drug delivery applications.* Materials Today: Proceedings, 2020. **28**: p. 1460-1466.
9. Kolanthai, E., et al., *Agarose encapsulated mesoporous carbonated hydroxyapatite nanocomposites powder for drug delivery.* J Photochem Photobiol B, 2017. **166**: p. 220-231.
10. Chen, Y., et al., *Bioinspired fabrication of carbonated hydroxyapatite/chitosan nanohybrid scaffolds loaded with TWS119 for bone regeneration.* Chemical Engineering Journal, 2018. **341**: p. 112-125.
11. Dey, S., M. Das, and V.K. Balla, *Effect of hydroxyapatite particle size, morphology and crystallinity on proliferation of colon cancer HCT116 cells.* Mater Sci Eng C Mater Biol Appl, 2014. **39**: p. 336-9.
12. Zhang, Y., et al., *Three dimensional macroporous hydroxyapatite/chitosan foam-supported polymer micelles for enhanced oral delivery of poorly soluble drugs.* Colloids Surf B Biointerfaces, 2018. **170**: p. 497-504.
13. Rokia M Salama et al., P*reparation of biocompatible chitosan nanoparticles loaded with Aloe vera extract for use as a novel drug delivery mechanism to improve the antibacterial characteristics of cellulose-based fabrics.* Egyptian Journal of Chemistry, 2022, 65 (3), p.589-604
14. Avcu, E., et al., *Electrophoretic deposition of chitosan-based composite coatings for biomedical applications: A review.* Progress in Materials Science, 2019. **103**: p. 69-108.
15. He, J., et al., *Chitosan-coated hydroxyapatite and drug-loaded polytrimethylene carbonate/polylactic acid scaffold for enhancing bone regeneration.* Carbohydr Polym, 2021. **253**: p. 117198.
16. Wahba, S.M., A.S. Darwish, and S.M. Kamal, *Ceria-containing uncoated and coated hydroxyapatite-based galantamine*

nanocomposites for formidable treatment of Alzheimer's disease in ovariectomized albino-rat model. Mater Sci Eng C Mater Biol Appl, 2016. **65**: p. 151-63.
17. Prakash, J., et al., *Nanocomposite chitosan film 3.containing graphene oxide/hydroxyapatite/gold for bone tissue engineering.* Int J Biol Macromol, 2020. **154**: p. 62-71.
18. Shahraki, N., et al., *Preparation and characterization of PEGylated liposomal Doxorubicin targeted with leptin-derived peptide and evaluation of their anti-tumor effects, in vitro and in vivo in mice bearing C26 colon carcinoma.* Colloids Surf B Biointerfaces, 2021. **200**: p. 111589.
19. Wang, X., G. Wang, and Y. Zhang, *Research on the biological activity and doxorubicin release behavior in vitro of mesoporous bioactive SiO2-CaO-P2O5 glass nanospheres.* Applied Surface Science, 2017. **419**: p. 531-539.
20. Shang, S., et al., *Molecular dynamics simulation of the adsorption behavior of two different drugs on hydroxyapatite and Zn-doped hydroxyapatite.* Materials Science and Engineering: C, 2019. **105**: p. 110017.
21. Sredni, B., *Immunomodulating tellurium compounds as anti-cancer agents.* Semin Cancer Biol, 2012. **22**(1): p. 60-9.
22. Angeli, A., et al., *Tellurides bearing benzensulfonamide as carbonic anhydrase inhibitors with potent antitumor activity.* Bioorg Med Chem Lett, 2021. **45**: p. 128147.
23. Doering, M., et al., *Selenium- and tellurium-containing redox modulators with distinct activity against macrophages: possible implications for the treatment of inflammatory diseases.* Tetrahedron, 2012. **68**(51): p. 10577-10585.
24. Du, P., et al., *A new tellurium-containing amphiphilic molecule induces apoptosis in HCT116 colon cancer cells.* Biochim Biophys Acta, 2014. **1840**(6): p. 1808-16.
25. Scibior, A., et al., *Vanadium: Risks and possible benefits in the light of a comprehensive overview of its pharmacotoxicological mechanisms and multi-applications with a summary of further research trends.* J Trace Elem Med Biol, 2020. **61**: p. 126508.
26. Evangelou, A.M., *Vanadium_cancer_treatment_CritRevOncHem2002.pdf.* critical reviews in oncology/Hematology, 2002. **42**: p. 249-265.
27. Kim, H., et al., *Optimized Zn-doped hydroxyapatite/doxorubicin bioceramics system for efficient drug delivery and tissue engineering application.* Ceramics International, 2018. **44**(6): p. 6062-6071.
28. Agalya, P., et al., *Surfactant-assisted microwave synthesis of luminescent/magnetic bifunctional hydroxyapatite nanorods for dual-model imaging.* Optik, 2021. **225**: p. 165564.
29. Bulina, N.V., et al., *Features of solid-phase mechanochemical synthesis of hydroxyapatite doped by copper and zinc ions.* Journal of Solid State Chemistry, 2021. **296**: p. 121973.
30. Karthikeyan, P., et al., *Effective and selective removal of organic pollutants from aqueous solutions using 1D hydroxyapatite-decorated 2D reduced graphene oxide nanocomposite.* Journal of Molecular Liquids, 2021. **331**: p. 115795.
31. Cipreste, M.F., et al., *A new theranostic system for bone disorders: Functionalized folate-MDP hydroxyapatite nanoparticles with radiolabeled copper-64.* Materials Chemistry and Physics, 2020. **254**: p. 123265.
32. Liu, X., et al., *A novel thermo-sensitive hydrogel based on thiolated chitosan/hydroxyapatite/beta-glycerophosphate.* Carbohydr Polym, 2014. **110**: p. 62-9.
33. Karthikeyan, P., et al., *Hydrothermal synthesis of hydroxyapatite-reduced graphene oxide (1D–2D) hybrids with enhanced selective adsorption properties for methyl orange and hexavalent chromium from aqueous solutions.* Chemosphere, 2021. **276**: p. 130200.
34. Dhatchayani, S., et al., *Effect of curcumin sorbed selenite substituted hydroxyapatite on osteosarcoma cells: An in vitro study.* Journal of Drug Delivery Science and Technology, 2020. **60**: p. 101963.
35. Kim, H.S., et al., *Therapeutic tissue regenerative nanohybrids self-assembled from bioactive inorganic core / chitosan shell nanounits.* Biomaterials, 2021. **274**: p. 120857.
36. Li, F., et al., *Near-infrared light stimuli-responsive synergistic therapy nanoplatforms based on the coordination of tellurium-containing block polymer and cisplatin for cancer treatment.* Biomaterials, 2017. **133**: p. 208-218.
37. Zhou, C., et al., *The sorption of single- and multi-heavy metals in aqueous solution using enhanced nano-hydroxyapatite assisted with ultrasonic.* Journal of Environmental Chemical Engineering, 2021. **9**(3): p. 105240.
38. Li, R., et al., *Pb(II) adsorption characteristics of magnetic GO-hydroxyapatite and the contribution of GO to enhance its acid resistance.* Journal of Environmental Chemical Engineering, 2021. **9**(4): p. 105310.
39. Yusoff, M.F., et al., *Physicochemical, antibacterial and biocompatibility assessments of silver incorporated nano-hydroxyapatite synthesized using a novel microwave-assisted wet*

precipitation technique. Materials Characterization, 2021: p. 111169.
40. Guo, Z., et al., *Versatile biomimetic cantharidin-tellurium nanoparticles enhance photothermal therapy by inhibiting the heat shock response for combined tumor therapy.* Acta Biomater, 2020. **110**: p. 208-220.
41. Nishikawa, M., et al., *Visible light responsive vanadium-substituted hydroxyapatite photocatalysts.* Journal of Photochemistry and Photobiology A: Chemistry, 2015. **311**: p. 30-34.
42. Guo, J., et al., *Nano vanadium dioxide films deposited on biomedical titanium: a novel approach for simultaneously enhanced osteogenic and antibacterial effects.* Artif Cells Nanomed Biotechnol, 2018. **46**(sup2): p. 58-74.
43. Dasireddy, V.D.B.C., H.B. Friedrich, and S. Singh, *Studies towards a mechanistic insight into the activation of n-octane using vanadium supported on alkaline earth metal hydroxyapatites.* Applied Catalysis A: General, 2013. **467**: p. 142-153.
44. Kundu, B., et al., *Doxorubicin-intercalated nano-hydroxyapatite drug-delivery system for liver cancer: An animal model.* Ceramics International, 2013. **39**(8): p. 9557-9566.